communications materials

Article

https://doi.org/10.1038/s43246-024-00594-1

Static magnetic order with strong quantum fluctuations in spin-1/2 honeycomb magnet $Na_2Co_2TeO_6$

Check for updates

Jinlong Jiao[1,14], Xiyang Li[2,14], Gaoting Lin[1,14] ✉, Mingfang Shu[1,3], Wei Xu[1], Oksana Zaharko[4], Toni Shiroka[5,6], Tao Hong[7], Alexander I. Kolesnikov[7], Guochu Deng[8], Sarah Dunsiger[9,10], Meigan C. Aronson[2], Haidong Zhou[11], Xiaoqun Wang[12], Tian Shang[13] ✉ & Jie Ma[1] ✉

Kitaev interactions, arising from the interplay of frustration and bond anisotropy, can lead to strong quantum fluctuations and, in an ideal case, to a quantum-spin-liquid state. However, in many nonideal materials, spurious non-Kitaev interactions typically promote a zigzag antiferromagnetic order in the *d*-orbital transition-metal compounds. Here, by combining neutron scattering with muon-spin rotation and relaxation techniques, we provide mechanism insights into the exotic properties of $Na_2Co_2TeO_6$, a candidate material of the Kitaev model. Below T_N, the zero-field muon-spin relaxation rate becomes almost constant (~0.45 μs^{-1}). We attribute this temperature-independent relaxation rate to the strong quantum fluctuations, as well as to the frustrated Kitaev interactions. As the magnetic field increases, neutron scattering data indicate a broader spin-wave excitation at the *K*-point. Therefore, quantum fluctuations seem not only robust but are even enhanced by the applied magnetic field. Our findings provide valuable hints for understanding the onset of the quantum-spin-liquid state in Kitaev materials.

The Kitaev model, describing a spin-1/2 two-dimensional (2D) honeycomb lattice as an exactly solvable 2D spin model that achieves a quantum-spin-liquid (QSL) ground state[1], has attracted considerable attention. Numerous theoretical and experimental attempts have been made in search for a QSL candidate with dominant bond-dependent anisotropic-exchange interactions K, namely, the Kitaev interactions[2–19]. To date, the Kitaev model has been successfully realized in several 3*d*, 4*d*, and 5*d* transition-metal families[8–13,18–22]. Unfortunately, owing to the ubiquitous presence of non-Kitaev interactions[6,7,13,15], e.g., Heisenberg exchanges, or off-diagonal symmetric interactions Γ and Γ', at low temperatures and in the absence of magnetic fields, most of these materials fail to realize a QSL state and exhibit instead a zigzag antiferromagnetic (AFM) order[6–13,18–22].

Compared to the previously discovered 4*d*/5*d* Ru/Ir systems, characterized by a strong spin-orbit coupling (SOC)[15–17,19], the 3*d* Co-based Kitaev QSL candidate materials remain highly controversial[12,13,20,23–29]. A good example of such materials is $Na_2Co_2TeO_6$ (NCTO), originally thought as one of the most promising cases for studying Kitaev physics[12,13,15,20,29–36]. Although the evidence of a field-induced QSL is available in NCTO[13,20,37,38], the magnetic structure of its ground state remains an open and intriguing question[13,20,27,28,32,34,39], whose answer should help to understand the role of the competitors of K, such as the nearest-neighbor (NN) Heisenberg coupling J_1 and the third NN Heisenberg coupling J_3.

Recently, by using various experimental methods, such as single-crystal or powder neutron diffraction, nuclear magnetic resonance, and electrical polarization measurements, researchers have attempted to understand the magnetic structure of NCTO[27,28,30–32,40,41], yet an undisputed conclusion has not been reached. i) Powder neutron diffraction experiments suggest a zigzag AFM order, with the magnetic moments lying in the *ab* plane [see Fig. 1a], accompanied by a Néel-type canting along the *c* axis below $T_N \sim 26$ K[40,41]. However, single-crystal neutron diffraction suggests a triple-q order (or multi-k structure) in the absence of a magnetic field[12,28,29,32]. ii) Although the field dependence of the characteristic magnetic reflections (0.5, 0, 1) and (0, 0.5, 1) demonstrates the magnetic multi-domain effect of the zigzag AFM order[28], the temperature dependence of the (0.5, 0, 0) magnetic reflection cannot rule out a triple-q order[12,28,32]. iii) The spin dynamics were analyzed by a generalized Heisenberg–Kitaev model with five symmetry-allowed terms: K, Γ and Γ', J_1, and J_3[13,34–36,42], and two different exchange frustrations: Kitaev and J_1-J_3. However, such a complex model made the determination of the ground state rather difficult. To distinguish the two possible magnetic structures, i.e., multi-domain or multi-k, a good strategy consists in measuring the field- and temperature-dependent magnetic reflections and the related dynamics at the M-points lying in the *ab*-plane, such as M (0.5, 0, L), M_1 (−0.5, 0.5, L), and M_2(0, 0.5, L), where L is an arbitrary integer [see Fig. 1b].

A full list of affiliations appears at the end of the paper. ✉e-mail: doublewood@sjtu.edu.cn; tshang@phy.ecnu.edu.cn; jma3@sjtu.edu.cn

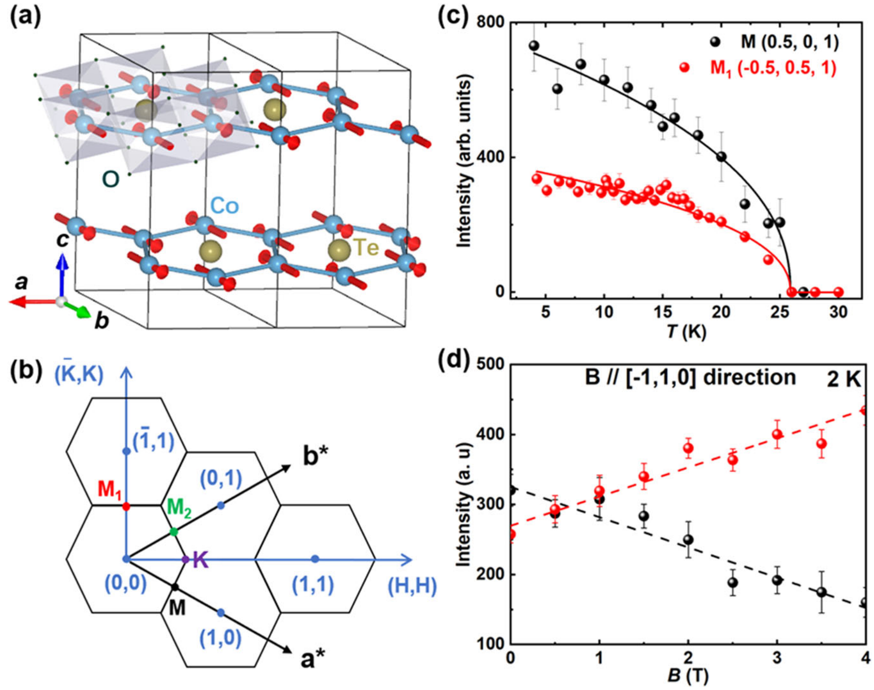

Fig. 1 | The honeycomb structure and single-crystal neutron diffraction for NCTO. **a** Magnetic structure of NCTO. **b** Schematic plots of the Brillouin zones showing the in-plane high symmetry points M, M_1, M_2, and K denoted by black, red, green, and purple dots, respectively. The high symmetry points are identical for L with different integers along the c-axis. **c** The temperature dependence of the zero-field intensity of two magnetic reflections at M (0.5, 0, 1) and M_1 (−0.5, 0.5, 1). The solid lines represent the fits to a phenomenological model (see details in the text). **d** Field-dependent intensity of magnetic reflections at M and M_1 points, collected at T = 2 K and with the magnetic field applied along the [−1, 1, 0] direction. Dashed lines are guides to the eyes. The error bars are 95% confidence intervals of the Gaussian fit.

In this paper, we investigate the magnetic order and dynamics of NCTO single crystals via neutron scattering and muon-spin rotation and relaxation (μSR) techniques. Changes of the characteristic magnetic reflections of M (0.5, 0, 1) and M_1 (−0.5, 0.5, 1) with temperature and magnetic field indicate that the magnetic ground state has a multi-domain structure, rather than a multi-k structure. Below T_N, the modulation of the magnetic domains induces two other transitions at T_F and T^*, reflected also by the temperature-dependent weak transverse-field (wTF) μSR asymmetry. Furthermore, the estimated static magnetic volume fraction (~90%) confirms the homogeneous nature of the ordering of NCTO single crystals. The relatively large and temperature-independent muon-spin relaxation rate in the AFM state suggests the presence of strong quantum spin fluctuations in NCTO.

Results and discussion

Single-crystal neutron diffraction

To determine whether the magnetic ground state of NCTO is a multi-domain structure or a multi-k structure, both the temperature- and magnetic-field dependence of the magnetic reflections M (0.5, 0, 1) and M_1 (−0.5, 0.5, 1) were measured for the wave vectors k = (0.5, 0, 0) and (−0.5, 0.5, 0), respectively [see Fig. 1c, d]. The integrated intensity was calculated by fitting the raw data with a Gaussian function, as illustrated in Fig. S1 of the Supplementary materials. The differences in the non-normalized scattering intensity at the M and M_1 points may be due to the non-spherical sample morphology (see sample photo in Fig. S1 of Supplemental materials). The temperature-dependent intensity curves $I(T)$ at both M and M_1 points can be well fitted using a phenomenological model: $I(T) = I_0 \cdot [1-(T/T_N)]^{2\beta}$[43], yielding a magnetic ordering temperature $T_N \approx 26$ K and $\beta \approx 0.22$. The $I(T)$ curves for both M and M_1 show similar behaviors, but a small bump near $T_F \approx 15$ K only appears for the M_1 point, implying that the anomaly at T_F may not be attributed to a magnetic phase transition. Interestingly, the spin-wave-excitation gap at the M-point which is ~1 meV vanishes at a temperature close to $T_F = 15$ K ~ 1.3 meV[32]. Furthermore, the appearance of spin-wave-excitation gap can be attributed to the SOC inducing magnetic anisotropic-exchange interactions K and Γ terms in NCTO[13]. Therefore, the weak anomaly at T_F can be interpreted as the modulation of anisotropy. Apparently, the M_1 point is responsive to variations in anisotropy, whereas the M point is not. This implies that the ground-state magnetic structure is not a multi-k structure, as such a structure would require the various arms of the k vector to respond uniformly to the external perturbations[44–48]. Hence, the subtle differences between these two magnetic reflections indicate that the magnetic ground state is a multi-domain structure, that is, the domains corresponding to the k vectors of (0.5, 0, 0) and (−0.5, 0.5, 0) are not equally populated. In addition, the estimated $\beta \approx 0.22$ is neither consistent with the ideal 2D Ising ($\beta = 0.125$) nor the 3D Ising ($\beta = 0.326$) system[49], but it is more consistent with quasi-2D magnetic correlations[13,20,32].

As shown in Fig. 1d, the multi-domain structure is further supported by the field-dependent intensity $I(B)$ at the magnetic reflections M and M_1 for **B** // [−1, 1, 0]. The M and M_1 reflections exhibit completely opposite field dependence. When increasing the magnetic field, the intensity of the M reflection decreases, while that of M_1 increases. Such opposite field dependence implies that the macroscopic symmetry is broken by the applied magnetic field and, thus, that the magnetic domains along the field direction gradually grow, while the domains in other directions are suppressed[44]. With the application of an external constraint (magnetic field or uniaxial stress), each arm of the k vector would exhibit a different response in the case of a multi-domain scenario, while they would show similar behavior in the case of a multi-k scheme[45–48]. Clearly, our neutron data support a multi-domain structure rather than a multi-k structure in NCTO single crystal. It is worth mentioning that, in the zigzag AFM state, NCTO exhibits a twofold symmetry in the angular dependence of the magnetic torque[20], which might be related to the different $I(B)$ field responses at the magnetic reflections M and M_1.

Inelastic neutron scattering

Another feature of quantum fluctuations in certain strong quantum magnets is a broadening of the spin-wave-excitation spectra[50–52]. To search for the quantum fluctuations in an external magnetic field, we performed single-crystal inelastic-neutron-scattering measurements by applying various magnetic fields up to 4 T along the [−1,1,0] direction. As shown in Fig. 2a, b, a spin-wave band can be identified at 0 and 4 T along the high symmetry momentum directions Γ-K-M (see the arrows in the inset of Fig. 2). As expected, in the zero-field case, the gapped magnon band at the M-point reaches the minimum energy value and has the largest intensity, thus supporting a zigzag AFM order driven by the non-Kitaev interactions[12,20]. The spin-wave band at 4 T shows similar features to the lowest-energy spin-wave-excitation spectra at 0 T [see Fig. 2b], but it is significantly broadened by the external field. Note that, in NCTO, we do not

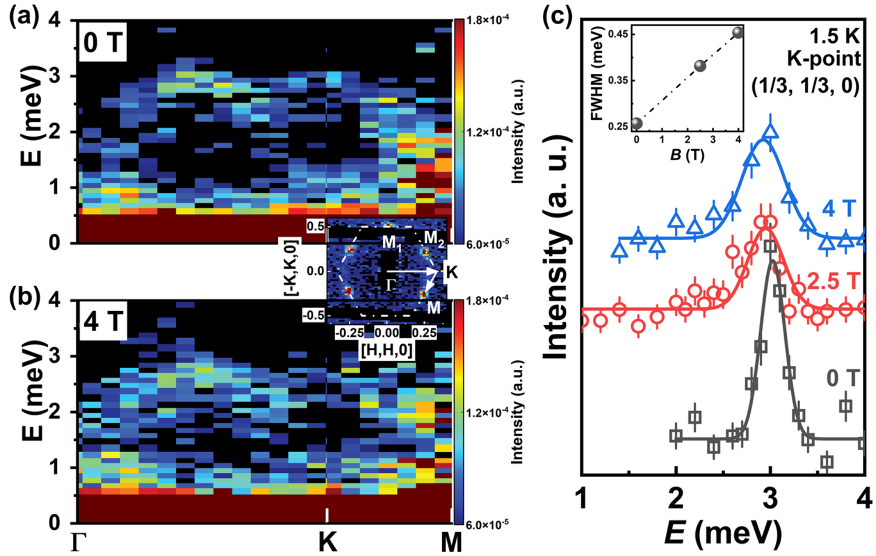

Fig. 2 | Single-crystal inelastic neutron scattering results for NCTO. a, b Lowest-energy spin-wave-excitation spectra at 2 K in the magnetic fields of 0 T and 4 T, respectively. The color bars indicate the scattering intensity in a linear scale. The inset shows the elastic neutron scattering plot which is integrated at the elastic location 00 L = [−2.5, 2.5] r.l.u. and E = [−0.075, 0.075] meV at 0 T using a fixed incident energy E_i = 60 meV. The white dash-dotted lines represent the Brillouin zone boundaries. The high symmetry points Γ, K, M, M_1 and M_2 are marked, and the white arrows show the high symmetry momentum directions Γ-K-M path in the inset. **c** The constant-Q scans of the K-point (1/3, 1/3, 0) collected at T = 1.5 K by applying magnetic fields up to 4 T along the [−1,1,0] direction. The solid lines represent the fits using a Gaussian function. The error bars are the standard deviation of the inelastic neutron scattering experimental data. The inset shows the field dependence of the FWHM of the excitation gap.

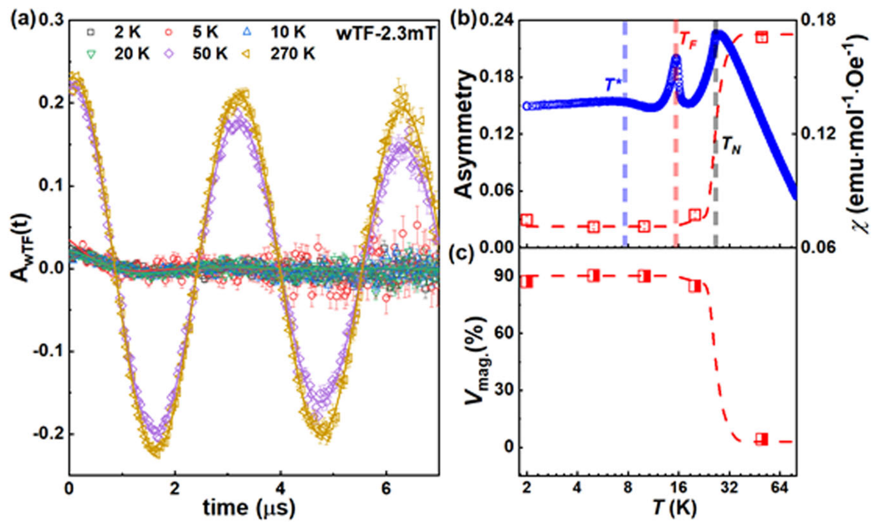

Fig. 3 | Magnetic phase transition and magnetic volume fraction of NCTO, as measured by wTF-μSR. a Time-domain wTF-μSR spectra collected at different temperatures in a weak transverse field of 2.3 mT, acquired at the M20D beamline. The error bars are the standard error of the mean. Solid lines are the fit results utilizing Eq. (1). To highlight the low-amplitude oscillations below T_N, the respective time-domain wTF-μSR spectra are also plotted in Fig. S7 of supplemental materials. **b** The temperature-dependent A_{NM} asymmetry (left axis and red symbols) was obtained from fits of the wTF-μSR data. The error bars represent the standard deviation of the fit parameters. For a comparison, we present the zero-field cooling (ZFC) magnetic susceptibility curve $\chi(T)$ measured at B = 0.01 T (right axis and blue symbols) with **B** // a^*-axis. The magnetic susceptibility data were taken from ref. 20. **c** The estimated magnetic volume fraction versus temperature. The red dashed lines in (**b**) and (**c**) are guides for the eyes.

observe a splitting of the spin-wave band into multiple branches under an applied magnetic field. Hence, such broadening is most likely caused by the field-induced quantum fluctuations, which can be further evidenced by constant-Q scans at the K-point. As shown in Fig. 2c, at 0 T, the excitation gap is centered around 3 meV[12,20]. Upon increasing the magnetic field to 4 T, the zigzag AFM order is still present [see $I(B)$ curves in Fig. 1d], but the excitation broadens continuously. The full width at half maximum (FWHM) of the excitation vs the magnetic field is shown in the inset of Fig. 2c. These results indicate that quantum fluctuations in NCTO are enhanced by an applied magnetic field. This is highly consistent with the field-induced magnetically disordered state with strong quantum fluctuations observed between 7.5 and 10 T with **B** // a^*-axis and such strong quantum fluctuations are more intuitively reflected in our μSR data[13,20,38].

Muon-spin rotation and relaxation

As an extremely sensitive probe of complex quantum magnetism, μSR is regularly used to investigate the magnetic order and dynamics at a microscopic level. Here, the combination of a long-range (neutron scattering) and a short-range (μSR) technique helped us to confirm the multi-domain magnetic structure and the quantum fluctuations in a NCTO single crystal.

The analysis of wTF-μSR spectra allowed us to establish the temperature evolution of the magnetic volume fraction and to determine the magnetic transition temperatures. Here, an external field of B = 2.3 mT, applied perpendicular to the initial muon-spin direction, leads to a precession of the muon spins with a frequency $\gamma_\mu B$ (where $\gamma_\mu/2\pi$ = 135.53 MHz/T is the muon's gyromagnetic ratio), as shown in Fig. 3a. Note that a field of 2.3 mT is much smaller than the internal fields created by the long-range magnetically ordered state in the NCTO single crystal (see Fig. 4). Therefore, the muon-spin precession reflects only the non-magnetic part of the sample, since in its long-range magnetically order state NCTO exhibits a very fast muon-spin depolarization, here, in less than a few tenths of μs. Consequently, without considering this very fast relaxation, the wTF-μSR spectra can be described by the function:

$$\mathrm{A}_{wTF}(t) = A_{NM}\cos(\gamma_\mu B_{\mathrm{int}} \cdot t + \varphi)e^{-\lambda t}, \quad (1)$$

where A_{NM} is the initial muon-spin asymmetry reflecting the muons implanted in the nonmagnetic (NM) or paramagnetic (PM) fraction of NCTO single crystal; B_{int} is the local field sensed by muons (here almost identical to the applied magnetic field); φ is an initial phase and λ is the muon-spin relaxation rate.

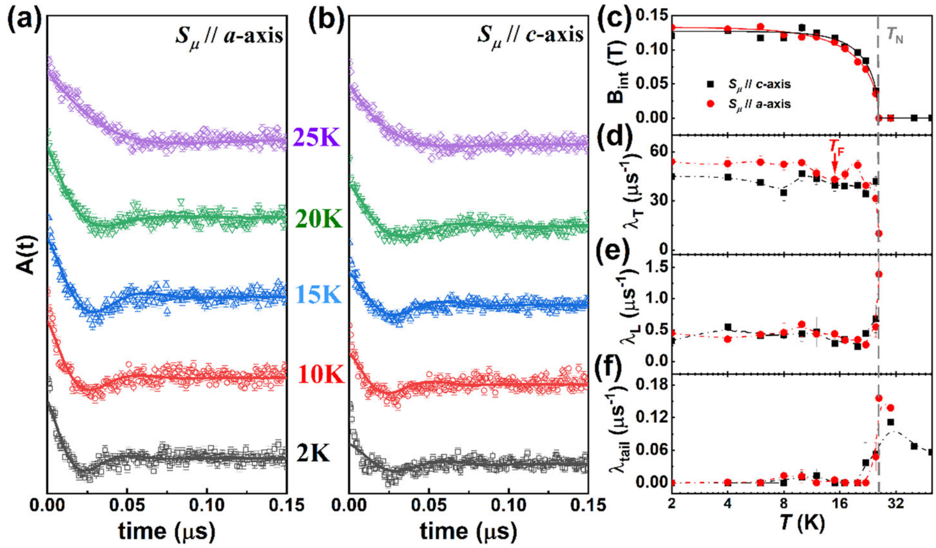

Fig. 4 | Zero-field μSR spectra of NCTO. a, b Zero-field (ZF) μSR time spectra measured at selected temperatures (displaced vertically for clarity) with the muon-spin direction $\mathbf{S}_\mu$ // a and c-axis, respectively. Data were taken on the M20D channel at TRIUMF. The error bars are the standard error of the mean. The solid curves represent fits to Eq. (2). **c**–**f** Temperature dependence of the $B_{\rm int}$, $\lambda_{\rm T}$, $\lambda_{\rm L}$, and $\lambda_{\rm tail}$, respectively, as derived from the analysis of ZF-μSR. The error bars represent the standard deviation of the fit parameters. The magnetic ordering temperature is $T_{\rm N} \approx 26$ K and is consistent with magnetic susceptibility data. Solid lines in panels (**c**) are fits using a phenomenological equation described in the text; dash-dotted lines in panels (**d**–**f**) are guides to the eyes.

Figure 3b presents the temperature dependence of the asymmetry for the wTF-μSR spectra. Below $T_{\rm N}$, a static spin component leads to a fast reduction of asymmetry. Hence, $A_{\rm NM}$ starts to decrease quickly as one approaches the AFM ordering temperature, consistently with the magnetic susceptibility data. Another broad and weak peak was observed in the wTF-5mT data at temperatures close to $T_{\rm F}$ during an independent experiment (see Fig. S3 of Supplemental materials). Although NCTO undergoes three successive AFM transitions [indicated by dashed lines in Fig. 3b], the $A_{\rm NM}(T)$ curve does not capture the possible phase transition at T^*[13]. In the case of a fully magnetically ordered material, the magnetic volume fraction $V_{\rm mag}$ at temperatures below the magnetic ordering temperature is close to 100%[53,54]. Here, the temperature dependence of the magnetic volume fraction was estimated from $V_{\rm mag}(T) = 1 - A_{\rm NM}(T)/A_{\rm NM}\ (T > T_{\rm N})$ [see Fig. 3c]. In our case, the static magnetic volume fraction is up to 90% and possible spin-glass behavior, typically revealed by ac susceptibility measurements, is absent in our NCTO single crystal[27]. These results indicate that, below $T_{\rm N}$, NCTO can be considered as fully magnetically ordered, ruling out heterogeneous behavior.

If the electronic magnetic moments fluctuate very fast (typically above 10^{12} Hz in the PM state), the muon-spin polarization would not be influenced. When the system starts to enter the magnetically ordered state, such fluctuations slow down significantly. This scenario gives rise to a fast depolarization with superimposed oscillations, reflected in the appearance of static magnetic moments and the coherent precession of the muon-spin polarization, respectively. Figure 4a, b shows the ZF-μSR time spectra for both $\mathbf{S}_\mu$ // a and $\mathbf{S}_\mu$ // c-axis (see also Fig. S4 of Supplementary materials). Such fast depolarization (within 50 ns) with superimposed oscillations below $T_{\rm N}$, has been observed in other antiferromagnets with strong frustration[54,55], thus suggesting that the exotic frustrated state in NCTO might originate from the Kitaev-type frustration[13,34–36,42]. To track the evolution of the muon asymmetry across the whole temperature range, the ZF-μSR spectra were modeled by:

$$A_{ZF}(t) = A_1 \cdot [\alpha \cos(\gamma_\mu B_{\rm int} t + \varphi) \cdot e^{-\lambda_T t} + (1-\alpha) \cdot e^{-\lambda_L t}] + A_2 e^{-\lambda_{tail} t} \cdot G_{KT}. \quad (2)$$

Here, α and $1-\alpha$ are the oscillating (i.e., transverse) and non-oscillating (i.e., longitudinal) fractions of the μSR signal, λ_T and λ_L represent the transverse and longitudinal muon-spin relaxation rates, A_1 and A_2 represent the asymmetries of two nonequivalent muon-stopping sites. The muons stopping at the second site do not undergo any precession but show only a weak relaxation, which can be described by an exponential relaxation $\lambda_{\rm tail}$. The ZF-μSR spectra show only a weak relaxation at temperatures above $T_{\rm N}$. Here, $G_{\rm KT}$ is the static Kubo-Toyabe relaxation function, normally used to describe the muon-spin relaxation due to the nuclear moments. In the magnetically ordered state, the muon-spin relaxation due to the electronic moments is significantly larger than the contribution from the nuclear moments. Therefore, below $T_{\rm N}$, the $G_{\rm KT}$ term can be safely ignored. In our analysis, we set $G_{\rm KT}$ to 1 at temperatures below $T_{\rm N}$ (see details in Fig. S5 of Supplemental materials).

Usually, changes in the magnitude of the magnetic moment can be detected by the temperature-dependent internal magnetic field $B_{\rm int}$(T). However, the modulation of magnetic domains is related to the distribution of internal magnetic fields. The fit parameters of the ZF-μSR spectra, here summarized in Fig. 4c–f, help us to distinguish the origin of these complex magnetic orders. It is worth mentioning that, as the temperature changes, α was allowed to vary, to ensure a more reasonable parameter set below $T_{\rm N}$. Indeed, the complex competition between the two different exchange frustrations of Kitaev- and J_1-J_3-type[13,34–36,42], can trigger significant spin fluctuations accompanied by changes in spin directions, as shown in Fig. S6c of Supplemental materials. The temperature-dependent parameter α shows weak anomalies near $T_{\rm F}$, most likely indicating that the modulation of the magnetic domains and the change of electronic moment directions are moderate.

The $B_{\rm int}$(T) curves for $\mathbf{S}_\mu$ // a and $\mathbf{S}_\mu$ // c exhibit similar features [see Fig. 4c], reflecting the local ordered magnetic moment of the Co^{2+} ions and provide one distinct phase transition temperature $T_{\rm N}$. Both curves are consistent with the temperature evolution of the magnetic moments obtained from powder[40] and single-crystal neutron diffractions (see details in Fig. 1). A phenomenological equation $B_{\rm int}(T) = B_{\rm int}(T=0) \cdot [1-(T/T_N)^\gamma]^\delta$ describes very well the $B_{\rm int}$(T) curves shown in Fig. 4c. Here, $B_{\rm int}(T=0)$ is the internal magnetic field at 0 K, γ and δ are two empirical parameters. The fitted parameters are summarized in Table SI in the Supplementary materials.

Interestingly, a tiny anomaly was observed at $T_{\rm F}$ in the temperature-dependent $\lambda_{\rm T}$(T) curve with $\mathbf{S}_\mu$ // a. We recall that the decay rate $\lambda_{\rm T}$ reflects the width of the static magnetic field distribution at the muon-stopping site [see Fig. 4d]. The observed anomalies at $T_{\rm F}$ are consistent with previous magnetic susceptibility and neutron scattering results, and this might suggest a possibility of redistribution of the magnetic domains originating from three different k-vectors of the zigzag AFM order. Hence, the multi-domain structure is compatible with both the ZF-μSR results and the single-crystal neutron diffraction data.

Spin fluctuations can be traced by the longitudinal relaxation rate $\lambda_{\rm L}$. As shown in Fig. 4e, both $\lambda_{\rm L}(T)$ curves diverge near $T_{\rm N}$, but also drop significantly below $T_{\rm N}$, indicating that spin fluctuations are the strongest close to the onset of the AFM order. Such strong spin fluctuations were further confirmed by the longitudinal-field (LF) μSR measurements [see Fig. S8 of Supplemental materials]. In NCTO, λ_L becomes approximately constant (0.45 μs^{-1}) at low temperatures below T_N. In $YbMgGaO_4$, another promising QSL candidate material, similar T-independent behavior, with a low-temperature value of 0.3 μs^{-1}, has been suggested to reflect its very strong quantum fluctuations[56]. Hence, the temperature independence of λ_L might also indicate strong quantum fluctuations in NCTO as thermal fluctuations are almost absent at extremely low temperatures. Incidentally, below T_N, the temperature-dependent $\lambda_{tail}(T)$ is nearly zero [see Fig. 4f], here reflecting a simple exponential correction originating from the low background.

We now discuss the zigzag AFM ground state with a multi-domain structure, accompanied by strong quantum fluctuations in NCTO. By using the same fitted parameters, $T_N \approx 26$ K and $\beta \approx 0.22$, the power-law function $I(T) = I_0 \cdot [1-(T/T_N)]^{2\beta}$ gives similar $I(T)$ curves at the M and M_1 points [see Fig. 1c]. However, the small bump at T_F, corresponding to an opening of the spin-wave-excitation gap[32], was observed only in the $I(T)$ curve measured at the M_1 point. The absence of anomaly at T_F in the $I(T)$ curve of the M point is consistent with the scenario of multi-domain structure, wherein distinct domains exhibit different behaviors. The field-dependent intensities of the magnetic reflections further confirm that the magnetic domains oriented along the magnetic field direction grow, while those along other directions are suppressed. At the same time, the subtle feature observed in the $\lambda_T(T)$ curves is also consistent with previous results and might indicate a domain reorientation occurring at T_F, coinciding with the multi-domain scenario. Such consistent experimental observations support a multi-domain structure rather than a multi-k structure.

Based on the generalized Heisenberg–Kitaev model[13,20,29,34–36,42], many previous studies have revealed a complex competition between the two types of exchange frustrations: Kitaev and J_1-J_3, which may lead to strong quantum fluctuations in the ground state of NCTO. Such quantum fluctuations are clearly evidenced by our ZF-μSR measurements: (1) NCTO exhibits a very fast depolarization (within 50 ns), typical of strongly frustrated antiferromagnets[54,55] [Fig. 4a, b]; (2) The temperature independence of λ_L, here close to 0.45 μs^{-1} [Fig. 4e] at low temperatures, is similar to that observed in $FeTe_2O_5Br$, where strong spin fluctuations coexist with a fully magnetically ordered state[57]. Taken together, our μSR data indicate that the spin dynamics at low temperatures is strongly influenced by quantum effects[57], with the opening of a spin-wave-excitation gap below T_F further eliminating the contribution of thermal fluctuations[32]. The zero-field quantum fluctuations inevitably remind us of the recently reported field-induced Kitaev QSL between 7.5 T and 10 T in NCTO[13,20,27,38]. Further, the broadening at the K-point, where the FWHM gradually increases in a magnetic field [see inset in Fig. 2c], suggests that quantum fluctuations are enhanced by the applied magnetic fields. These results indicate that the applied magnetic fields could quickly suppress the magnetically ordered states and highlight the contribution of Kitaev interactions to quantum fluctuations.

Conclusions

In summary, we investigated both the magnetic structure and the ground-state dynamics in NCTO. Our most significant finding is that NCTO hosts a multi-domain zigzag AFM order with strong quantum fluctuations. Our results provide experimental evidence in favor of the Heisenberg–Kitaev model, where the coexistence of static magnetic order (from the non-Kitaev interactions) with dynamic quantum fluctuations (from the frustrated K term) suggests a highly frustrated magnetic structure.

Note added. While preparing the present manuscript, we noticed that μSR experiments, with a lower early-time resolution (here up to 50 ns), were presented independently[58].

Methods

Sample preparation and characterization

The measurements were performed on high-quality single crystals grown by the flux method, as described elsewhere in ref. 20.

Single-crystal neutron diffraction and inelastic neutron scattering

A piece of NCTO single crystal was used for the neutron diffraction experiments [see the inset in Fig. S1a of Supplemental materials], performed at the thermal single-crystal diffractometer ZEBRA at the Swiss Spallation Neutron Source SINQ, Paul Scherrer Institut (PSI), Switzerland. A neutron wavelength of 1.383 Å, obtained by a Ge monochromator, was used for all the measurements at ZEBRA. In-field data were collected using a lifting arm normal-beam geometry, where the crystal was inserted in a 10-T vertical magnet. The magnetic states of NCTO were investigated with **B** // [−1 1 0] (equivalent to a^*-axis). Spin-wave excitation spectra were measured using the SEQUOIA time-of-flight spectrometer at the Spallation Neutron Source, Oak Ridge National Laboratory, USA[59,60]. Measurements at 2 K with applied field $B = 0$ T and 4 T were performed by rotating the sample around the vertical axis (sample a*-axis) in steps of 1° with $E_i = 18$ meV with high energy resolution (ΔE) of 0.41 meV (full width at half maximum of the elastic peak). In order to subtract the background, the INS data were collected at 90 K. The constant-Q scans of the K-point (1/3, 1/3, 0) at 1.5 K with applied field B up to 4 T and **B** // [-1,1,0] direction were measured on the Cold Triple Axis Spectrometer SIKA at the ANSTO, Australia[61]. Data on SIKA were collected using a fixed final-energy mode with $E_f = 5.0$ meV, achieving a resolution of 0.13 meV.

μSR

The ZF-, LF-, and wTF-μSR experiments were performed on the M20D surface muon beamline at TRIUMF in Vancouver, Canada using the LAMPF spectrometer. In addition, wTF-μSR experiments were also carried out at the general-purpose surface-muon (GPS) instrument at the πM3 beamline of the Swiss muon source (SμS) at PSI in Villigen, Switzerland. For the experiments on the M20D surface muon beamline at TRIUMF, four layers of aligned NCTO crystals were positioned on aluminum backed mylar tape, Fig. S2a, b of Supplemental materials, with their c axis parallel to the incident muon spin direction. We aimed to study the temperature evolution of the magnetically ordered phase and the dynamics of spin fluctuations. For the experiments on the GPS instrument, since NCTO is thin and flat, we simply used two layers of crystals and then wrapped them with Kapton foil, Fig. S2c, d of Supplemental materials. The incident muon spin direction was always parallel to the c-axis of the crystal. The muon spin could be rotated into the ab-plane (TRAN mode) or be left along the c-axis (LONG mode). Based on the wTF-μSR data taken at TRIUMF, we could determine the temperature evolution of the magnetic volume fraction. For the wTF-μSR measurements, the applied magnetic field was perpendicular to the incident muon spin direction. All the μSR spectra were analyzed using the musrfit software package[62].

Data availability

The data that support the findings of this study are available from the corresponding authors upon request.

Received: 30 March 2024; Accepted: 31 July 2024;
Published online: 20 August 2024

References

1. Kitaev, A. Anyons in an exactly solved model and beyond. *Ann. Phys.* **321**, 2–111 (2006).
2. Jackeli, G. & Khaliullin, G. Mott insulators in the strong spin-orbit coupling limit: from Heisenberg to a quantum compass and Kitaev models. *Phys. Rev. Lett.* **102**, 017205 (2009).
3. Chaloupka, J., Jackeli, G. & Khaliullin, G. Kitaev-Heisenberg model on a honeycomb lattice: possible exotic phases in iridium oxides A_2IrO_3. *Phys. Rev. Lett.* **105**, 027204 (2010).
4. Xu, C. et al. Possible Kitaev quantum spin liquid state in 2D materials with S=3/2. *Phys. Rev. Lett.* **124**, 087205 (2020).

5. Tanaka, O. et al. Thermodynamic evidence for a field-angle-dependent Majorana gap in a Kitaev spin liquid. *Nat. Phys.* **18**, 429–435 (2022).
6. Takagi, H., Takayama, T., Jackeli, G., Khaliullin, G. & Nagler, S. E. Concept and realization of Kitaev quantum spin liquids. *Nat. Rev. Phys.* **1**, 264–280 (2019).
7. Maksimov, P. A. & Chernyshev, A. L. Rethinking $\alpha-RuCl_3$. *Phys. Rev. Res.* **2**, 033011 (2020).
8. Yokoi, T. et al. Half-integer quantized anomalous thermal Hall effect in the Kitaev material candidate α-$RuCl_3$. *Science* **373**, 568–572 (2021).
9. Kasahara, Y. et al. Majorana quantization and half-integer thermal quantum Hall effect in a Kitaev spin liquid. *Nature* **559**, 227–231 (2018).
10. Banerjee, A. et al. Neutron scattering in the proximate quantum spin liquid α-$RuCl_3$. *Science* **356**, 1055–1059 (2017).
11. Hwan Chun, S. et al. Direct evidence for dominant bond-directional interactions in a honeycomb lattice iridate Na_2IrO_3. *Nat. Phys.* **11**, 462–466 (2015).
12. Yao, W., Iida, K., Kamazawa, K. & Li, Y. Excitations in the Ordered and Paramagnetic States of Honeycomb Magnet $Na_2Co_2TeO_6$. *Phys. Rev. Lett.* **129**, 147202 (2022).
13. Lin, G. et al. Field-induced quantum spin disordered state in spin$-1/2$ honeycomb magnet $Na_2Co_2TeO_6$. *Nat. Commun.* **12**, 5559 (2021).
14. Broholm, C. et al. Quantum spin liquids. *Science* **367**, 263 (2020).
15. Liu, H., Chaloupka, J. & Khaliullin, G. Kitaev spin liquid in 3d transition metal compounds. *Phys. Rev. Lett.* **125**, 047201 (2020).
16. Sano, R., Kato, Y. & Motome, Y. Kitaev-Heisenberg Hamiltonian for high-spin d^7 Mott insulators. *Phys. Rev. B.* **97**, 014408 (2018).
17. Liu, H. & Khaliullin, G. Pseudospin exchange interactions in d^7 cobalt compounds: Possible realization of the Kitaev model. *Phys. Rev. B.* **97**, 014407 (2018).
18. Kitagawa, K. et al. A spin-orbital-entangled quantum liquid on a honeycomb lattice. *Nature* **554**, 341–345 (2018).
19. Ma, J. Spins don't align here. *Nat. Phys.* **19**, 922–923 (2023).
20. Lin, G. et al. Evidence for field induced quantum spin liquid behavior in a spin$-1/2$ honeycomb magnet. *Res. Square*. https://doi.org/10.21203/rs.3.rs-2034295/v1 (2022).
21. Do, S.-H. et al. Majorana fermions in the Kitaev quantum spin system α-$RuCl_3$. *Nat. Phys.* **13**, 1079–1084 (2017).
22. Choi, S. K. et al. Spin waves and revised crystal structure of honeycomb iridate Na_2IrO_3. *Phys. Rev. Lett.* **108**, 127204 (2012).
23. Halloran, T. et al. Geometrical frustration versus Kitaev interactions in $BaCo_2(AsO_4)_2$. *Proc. Natl. Acad. Sci. USA* **120**, e2215509119 (2023).
24. Zhang, X. et al. A magnetic continuum in the cobalt-based honeycomb magnet $BaCo_2(AsO_4)_2$. *Nat. Mater.* **22**, 58–63 (2023).
25. Winter, S. M. Magnetic couplings in edge-sharing high-spin d^7 compounds. *J. Phys. Mater.* **5**, 045003 (2022).
26. Li, X. et al. Giant Magnetic In-Plane Anisotropy and Competing Instabilities in $Na_3Co_2SbO_6$. *Phys. Rev. X.* **12**, 041024 (2022).
27. Zhang, S. et al. Electronic and magnetic phase diagrams of the Kitaev quantum spin liquid candidate $Na_2Co_2TeO_6$. *Phys. Rev. B.* **108**, 064421 (2023).
28. Yao, W. et al. Magnetic ground state of the Kitaev $Na_2Co_2TeO_6$ spin liquid candidate. *Phys. Rev. Res.* **5**, L022045 (2023).
29. Kruger, W. G. F., Chen, W., Jin, X., Li, Y. & Janssen, L. Triple-q Order in $Na_2Co_2TeO_6$ from proximity to hidden-SU(2)-symmetric point. *Phys. Rev. Lett.* **131**, 146702 (2023).
30. Xiao, G., Xia, Z., Song, Y. & Xiao, L. Magnetic properties and phase diagram of quasi-two-dimensional $Na_2Co_2TeO_6$ single crystal under high magnetic field. *J. Phys. Condens. Matter.* **34**, 075801 (2021).
31. Lee, C. H. et al. Multistage development of anisotropic magnetic correlations in the Co-based honeycomb lattice $Na_2Co_2TeO_6$. *Phys. Rev. B.* **103**, 214447 (2021).
32. Chen, W. et al. Spin-orbit phase behavior of $Na_2Co_2TeO_6$ at low temperatures. *Phys. Rev. B.* **103**, L180404 (2021).
33. Yao, W. & Li, Y. Ferrimagnetism and anisotropic phase tunability by magnetic fields in $Na_2Co_2TeO_6$. *Phys. Rev. B.* **101**, 085120 (2020).
34. Kim, C. et al. Antiferromagnetic Kitaev interaction in $J_{eff}=1/2$ cobalt honeycomb materials $Na_3Co_2SbO_6$ and $Na_2Co_2TeO_6$. *J. Phys. Condens. Matter.* **34**, 045802 (2022).
35. Samarakoon, A. M., Chen, Q., Zhou, H. & Garlea, V. O. Static and dynamic magnetic properties of honeycomb lattice antiferromagnets $Na_2M_2TeO_6$, M=Co and Ni. *Phys. Rev. B.* **104**, 184415 (2021).
36. Songvilay, M. et al. Kitaev interactions in the Co honeycomb antiferromagnets $Na_3Co_2SbO_6$ and $Na_2Co_2TeO_6$. *Phys. Rev. B* **102**, 224429 (2020).
37. Hong, X. et al. Strongly scattered phonon heat transport of the candidate Kitaev material $Na_2Co_2TeO_6$. *Phys. Rev. B.* **104**, 144426 (2021).
38. Pilch, P. et al. Field- and polarization-dependent quantum spin dynamics in the honeycomb magnet $Na_2Co_2TeO_6$: magnetic excitations and continuum. *Phys. Rev. B* **108**, L140406 (2023).
39. Li, N. et al. Magnon-polaron driven thermal Hall effect in a Heisenberg-Kitaev antiferromagnet. *Phys. Rev. B* **108**, L140402 (2023).
40. Bera, A. K., Yusuf, S. M., Kumar, A. & Ritter, C. Zigzag antiferromagnetic ground state with anisotropic correlation lengths in the quasi-two-dimensional honeycomb lattice compound $Na_2Co_2TeO_6$. *Phys. Rev. B* **95**, 094424 (2017).
41. Lefrançois, E. et al. Magnetic properties of the honeycomb oxide $Na_2Co_2TeO_6$. *Phys. Rev. B* **94**, 214416 (2016).
42. Sanders, A. L. et al. Dominant Kitaev interactions in the honeycomb materials $Na_3Co_2SbO_6$ and $Na_2Co_2TeO_6$. *Phys. Rev. B.* **106**, 014413 (2022).
43. Garlea, V. O. et al. Magnetic and orbital ordering in the spinel MnV_2O_4. *Phys. Rev. Lett.* **100**, 066404 (2008).
44. Rodríguez-Carvajal, J. & Villain, J. Magnetic structures. *C. R. Physique* **20**, 770–802 (2019).
45. Saito, H. et al. In-plane anisotropy of single-q and multiple-q ordered phases in the antiferromagnetic metal $CeRh_2Si_2$. *Phys. Rev. B* **108**, 094440 (2023).
46. Khanh, N. D. et al. Zoology of multiple-Q spin textures in a centrosymmetric tetragonal magnet with itinerant electrons. *Adv. Sci.* **9**, 2105452 (2022).
47. Takagi, R. et al. Multiple-q noncollinear magnetism in an itinerant hexagonal magnet. *Sci. Adv.* **4**, eaau3402 (2018).
48. Park, P. et al. Tetrahedral triple-Q magnetic ordering and large spontaneous Hall conductivity in the metallic triangular antiferromagnet $Co_{1/3}TaS_2$. *Nat. Commun.* **14**, 8346 (2023).
49. Collins, M. F. *Magnetic Critical Scattering* (ed Lovesey, S. W.) (Oxford Univ. Press, 1989).
50. Ma, J. et al. Static and dynamical properties of the spin-1/2 equilateral triangular-lattice antiferromagnet $Ba_3CoSb_2O_9$. *Phys. Rev. Lett.* **116**, 087201 (2016).
51. Shen, Y. et al. Evidence for a spinon Fermi surface in a triangular-lattice quantum-spin-liquid candidate. *Nature* **540**, 559–562 (2016).
52. Shen, Y. et al. Fractionalized excitations in the partially magnetized spin liquid candidate $YbMgGaO_4$. *Nat. Commun.* **9**, 4138 (2018).
53. Zhu, X. Y. et al. Spin order and fluctuations in the $EuAl_4$ and $EuGa_4$ topological antiferromagnets: A μSR study. *Phys. Rev. B* **105**, 014423 (2022).
54. Rovers, M. T. et al. Muon-spin-relaxation investigation of the spin dynamics of geometrically frustrated chromium spinels. *Phys. Rev. B* **66**, 174434 (2002).
55. Kenney, E. M. et al. Novel magnetic ordering in $LiYbO_2$ probed by muon spin relaxation. *Phys. Rev. B* **106**, 144401 (2022).
56. Li, Y. et al. Muon spin relaxation evidence for the U(1) quantum spin-liquid ground state in the triangular antiferromagnet $YbMgGaO_4$. *Phys. Rev. Lett.* **117**, 097201 (2016).
57. Pregelj, M. et al. Persistent spin dynamics intrinsic to amplitude-modulated long-range magnetic order. *Phys. Rev. Lett.* **109**, 227202 (2012).

58. Miao, P. et al. Persistent spin dynamics in magnetically ordered honeycomb cobalt oxides. *arXiv*: 2307.16451v1 (2023).
59. Stone, M. B. et al. A comparison of four direct geometry time-of-flight spectrometers at the Spallation Neutron Source. *Rev. Sci. Instrum.* **85**, 045113 (2014).
60. Granroth, G. E. et al. SEQUOIA: a newly operating chopper spectrometer at the SNS. *J. Phys. Conf. Ser.* **251**, 012058 (2010).
61. Wu, C. M. et al. SIKA—the multiplexing cold-neutron triple-axis spectrometer at ANSTO. *J. Inst.* **11**, P10009 (2016).
62. Suter, A. & Wojek, B. M. Musrfit: a free platform-independent framework for μSR data analysis. *Phys. Procedia.* **30**, 69–73 (2012).

Acknowledgements

G.T.L., T.S., and J.M. thank the financial support from the National Key Research and Development Program of China (No. 2022YFA1402702), the National Natural Science Foundation of China (Nos. U2032213, 12004243, 12374105). G.T.L. acknowledges support from the Startup Fund for Young Faculty at SJTU (24×010500168). J.M. thanks the interdisciplinary program Wuhan National High Magnetic Field Center (No. WHMFC 202122), Huazhong University of Science and Technology. T.S. acknowledges support from the Natural Science Foundation of Shanghai (Grant Nos. 21ZR1420500 and 21JC1402300), Natural Science Foundation of Chongqing (Grant No. CSTB-2022NSCQ-MSX1678). X.Y.L. was supported by the National Science Foundation through grant NSF-DMR−1807451. Work at UBC (X.Y.L., M.C.A.) was supported by the Natural Sciences and Engineering Research Council of Canada (NSERC), and through the Stewart Blusson Quantum Matter Institute by the Canada First Research Excellence Fund (CFREF). M.S. thanks the support from Guangdong Provincial Key Laboratory of Extreme Conditions (Grant No. 2023B1212010002). The work performed in the University of Tennessee (crystal growth) was supported by NSF-DMR-2003117. We acknowledge the neutron beam time from SINQ with Proposal 20222504, SNS with Proposal No. IPTS-27393.1, and ANSTO with Proposal No. P15604. We thank ACNS for the beam time and the sample environment group at ACNS for the support. This research used resources at the Spallation Neutron Source, a DOE Office of Science User Facility operated by the Oak Ridge National Laboratory. Part of this work is based on experiments performed at the Swiss spallation neutron source SINQ, and the Swiss muon source at the Paul Scherrer Institut, Villigen, Switzerland.

Author contributions

J.J. and G.L. conceived the experimental measurements with supervision from J.M.; H.Z. and J.M. synthesized the crystalas. J.J. and O.Z. conducted the single crystal neutron scattering experiment, and J.J. processed the data. T.H., A.K., G.D., G.L., J.J., and J.M. carried out the inelastic neutron scattering experiment, with data analysis conducted by G.L., J.J., J.M., M.S., and X.W. Additionally, X.L., T.S., S.D., M.A., G.L., and J.M. performed the μSR experiment. X.L., G.L., T.S., and J.M. analyzed the μSR data. J.J. prepared the manuscript, with contributions from X.L., W.X., G.L., T.S., and J.M. All authors participated in discussions regarding the data and its interpretation.

Competing interests

The authors declare no competing interests.

Additional information

Supplementary information The online version contains supplementary material available at https://doi.org/10.1038/s43246-024-00594-1.

Correspondence and requests for materials should be addressed to Gaoting Lin, Tian Shang or Jie Ma.

Peer review information *Communications materials* thanks the anonymous reviewers for their contribution to the peer review of this work. Primary Handling Editor: Aldo Isidori. A peer review file is available.

Reprints and permissions information is available at http://www.nature.com/reprints

Publisher's note Springer Nature remains neutral with regard to jurisdictional claims in published maps and institutional affiliations.

[1]Key Laboratory of Artificial Structures and Quantum Control, Shenyang National Laboratory for Materials Science, School of Physics and Astronomy, Shanghai Jiao Tong University, Shanghai, China. [2]Department of Physics & Astronomy and Stewart Blusson Quantum Matter Institute, University of British Columbia, Vancouver, BC, Canada. [3]Guangdong Provincial Key Laboratory of Extreme Conditions, Dongguan, China. [4]Laboratory for Neutron Scattering and Imaging, Paul Scherrer Institut, Villigen, Switzerland. [5]Laboratory for Muon-Spin Spectroscopy, Paul Scherrer Institut, Villigen PSI, Switzerland. [6]Laboratorium für Festkörperphysik, ETH Zürich, Zürich, Switzerland. [7]Neutron Scattering Division, Oak Ridge National Laboratory, Oak Ridge, TN, USA. [8]Australian Centre for Neutron Scattering, Australian Nuclear Science and Technology Organization, Lucas Heights, NSW, Australia. [9]Department of Physics, Simon Fraser University, Burnaby, BC, Canada. [10]Centre for Molecular and Materials Science, TRIUMF, Vancouver, BC, Canada. [11]Department of Physics and Astronomy, University of Tennessee, Knoxville, TN, USA. [12]School of Physics, Zhejiang University, Hangzhou, China. [13]Key Laboratory of Polar Materials and Devices (MOE), School of Physics and Electronic Science, East China Normal University, Shanghai, China. [14]These authors contributed equally: Jinlong Jiao, Xiyang Li, Gaoting Lin.
✉e-mail: doublewood@sjtu.edu.cn; tshang@phy.ecnu.edu.cn; jma3@sjtu.edu.cn